Phase transformation of the intermetallic compound Al_4Ca

H. ZOGG*, P. SCHWELLINGER
Swiss Aluminium Ltd, Research and Development, CH-8212 Neuhausen am Rheinfall, Switzerland

By measurement of physical properties and microscopic examination it was found that the phase Al_4Ca undergoes a martensitic transformation with $M_s \simeq 130°$ C. The low temperature structure is monoclinic, $a = 0.6158$ nm, $b = 0.6175$ nm, $c = 1.118$ nm, $\beta = 88.9°$. The DI_3 structure ascribed to Al_4Ca hitherto is valid only above M_s. Orientation relationships indicate that the transformation proceeds by a shear of 1.1° on (1 1 0) planes of the DI_3 structure.

1. Introduction

According to Nowotny *et al.* [1], the structure of Al_4Ca at room temperature is supposed to be of DI_3 type (b c tetragonal) with $a = 0.4362$ nm and $c = 1.109$ nm. The structure was derived from a powder pattern by comparison with a known DI_3 type phase.

Only a few properties of Al_4Ca are known. The density ($\rho = 2.33\,g\,cm^{-3}$), hardness ($H_V \simeq 170$ to 200) and Young's modulus ($E = 3 \times 10^{10}\,N\,m^{-2}$), [2] are low compared to the corresponding properties of other intermetallic compounds, and it was concluded that the phase which forms peritectically at 700° C is not very stable [1].

Recently, Al–Al_4Ca eutectic alloys have received some attention as superplastic material [3, 4] and as microduplex alloys [5]. As these alloys contain $\simeq 30$ vol% Al_4Ca, a better understanding of the properties of Al_4Ca is desirable. Therefore we examined the behaviour of pure Al_4Ca. We found no anomalous deformation behaviour. The phase is completely brittle up to $\simeq 300°$ C, whereas above 400° C extensive plastic deformation was observed [6]. However, pronounced anomalies of physical properties were found at and below 130° C, indicating unknown phase transitions of Al_4Ca. These findings were the starting point of the present work.

2. Experimental procedure

Two types of samples were used for this study. The first type (type A) consisted of Al_4Ca prepared in massive form. Appropriate mixtures of 99.99% Al, and Ca pellets with a purity of > 99.5% (main impurity Mg according to the supplier) were melted under a KCl–NaCl flux and Ar, cast into a pre-heated iron mould, annealed under vacuum for several weeks at a few degrees below the peritectic temperature, and cooled down slowly to room temperature. The material still contained some Al and Al_2Ca due to incomplete peritectic reaction and compositional variations. Voids and microcracks were present, too (Fig. 1). For the chemical composition see Table I.

This type of sample was used for measurements of the specific heat, specific resistivity, thermal expansion and elasticity data. As we did not intend to give precise values of these properties, and as only the temperature variation of properties of the *same* sample are considered, the use of such imperfect material is justified.

For the second type of samples (type B), an

TABLE I Chemical composition of type A samples (wt%)

Ca	Cu	Fe	Mg	Si	Zn	Al
26.5	0.005	< 0.003	0.004	< 0.003	< 0.1	bal.

* Present address: Institut für technische Physik, ETH-Hönggerberg, CH-8093 Zürich Switzerland.

0022–2461/79/081923–10 $03.00/0

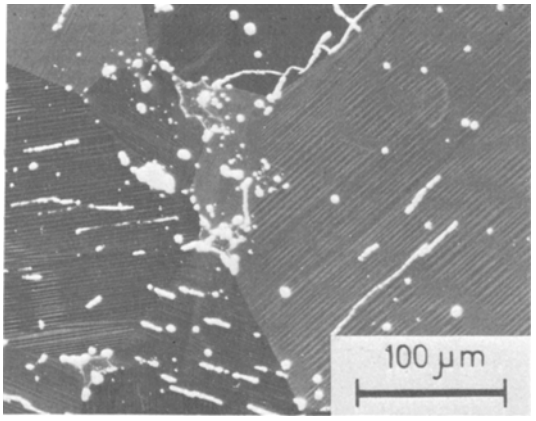

Figure 1 Internal structure of type A samples showing twin lamellae. The width of the microcracks and voids present is exaggerated due to the use of polarized light.

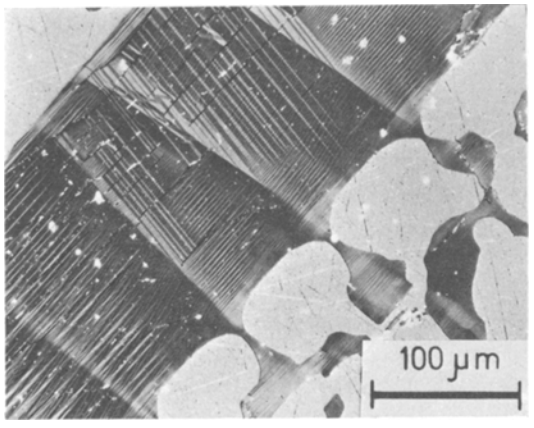

Figure 2 Internal structure of type B samples; primary Al_4Ca-plate surrounded by eutectic Al–Al_4Ca. (Polarized light).

Al–14 wt% Ca mixture (corresponding to the Ca-rich limit of the field of primary crystallization of Al_4Ca) was melted and cooled slowly (6 K min^{-1}) until the eutectic temperature was reached. Thus primary Al_4Ca platelets measuring up to $\simeq 0.5\,cm^2$ in area and $\simeq 0.3$ mm in thickness, surrounded by an Al–Al_4Ca eutectic, were obtained (Fig. 2). According to Laue patterns, the dominating faces of the Al_4Ca plates showed 4-fold symmetry. This type of sample was used for microscopic examination. Electron microscope (EM) samples of this type were much easier to prepare and handle than the extremely brittle type A samples. In most cases, the area that could be examined in the EM comprised one Al_4Ca particle only.

Some Al–14 wt% Ca material was remelted under Ar in high-purity graphite crucibles and lowered through a temperature gradient at a rate of 0.6 mm h^{-1}. Most of the primary Al_4Ca crystallized in massive form at the bottom of the crucible and nearly pure Al_4Ca could be separated. This sample was used for precision X-ray work.

The electrical resistivity was measured with a 4 pole, low frequency a.c. method using lock-in amplifier techniques. The samples were cut to $\simeq 5$ mm x 0.5 mm in cross-section and 5 mm in effective length; electrical contacts were made by springs. A programmable furnace or cryostat control was used and the $\rho(T)$–curves were plotted on a X–Y-recorder.

The specific heat was determined on $\simeq 50$ mg samples with a Perkin–Elmer differential scanning calorimeter (DSC II). The thermal expansion was measured with a "Dilatronic II" dilatometer (Theta Industries Inc.) using samples $\simeq 30\,mm^2$ in cross-section and 40 mm in length. Elastic data were obtained using pulse echo or resonance methods [7]*. Electron microscope work was performed on a Philips EM 300 microscope with an operating voltage of 100 kV.

3. Experimental results

3.1. Light microscopy

As Al_4Ca exhibits a pronounced optical anisotropy, orientational changes are easily resolved using polarized light. The heavily twinned internal structure visible in Figs. 1 and 2 shows at least 4 distinct orientation variants which are separated by straight boundaries in at least 5 different directions.

Using a heating stage, the internal structure of the Al_4Ca particles disappeared upon heating to $T \simeq 200°$ C and reappeared, but with different orientations, upon cooling back to room temperature. Samples annealed for 1 day at 160 and 90° C, respectively, and quenched into ice-water both showed the typical internal structure of Fig. 2.

3.2. Physical properties

The specific resistivity as a function of temperature is shown in Fig. 3a. A linear temperature dependence was observed between liquid nitrogen temperature and $\simeq -20°$ C and, also, above

* We thank Dr E. Török, Institut Straumann, Ch-4437 Waldenberg for carrying out these measurements.

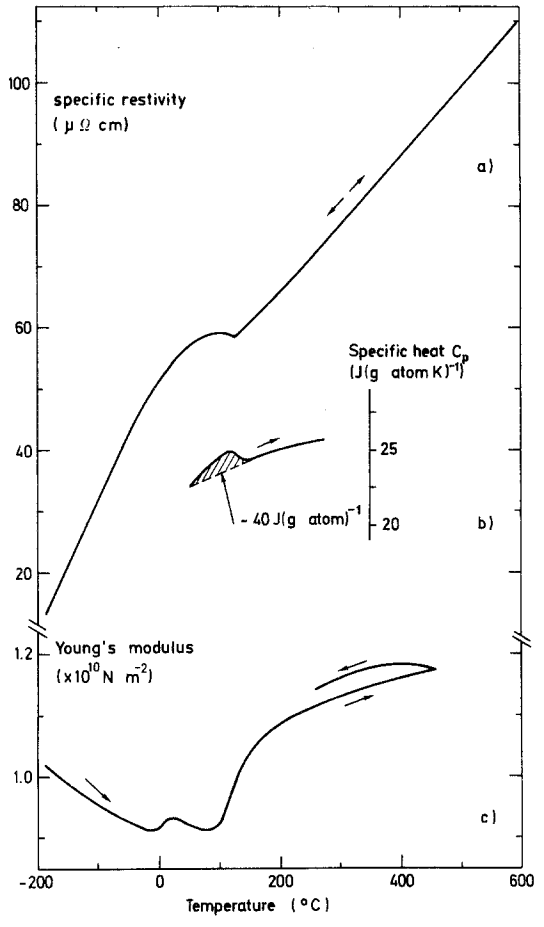

Figure 3 Temperature dependence of specific resistivity, specific heat (c_P) and Young's modulus of type A samples.

$\sim 130°$ C, but with a lower temperature coefficient. In the transition range the resistivity exhibits a flat maximum at $\simeq 100°$ C followed by a slight minimum at 130° C. Within the experimental scatter ($\pm 5°$ C) no hysteresis was detected on heating and cooling, using heating and cooling rates between 1 and 10 K min^{-1}. The measured shape of this curve indicating the occurrence of a phase transition may, in addition, be affected by the opening or closing of microcracks during the transformation, changing the effective dimensions of the sample. However, a deviation from linearity was observed with type B samples containing $\simeq 55$ vol% Al_4Ca in an Al matrix, the conductivity of which is 10 times higher than the type A samples. These also exhibited fewer microcrakcs, and the deviation was of the same kind as shown in Fig. 3a. Therefore we conclude that this deviation is real.

The specific heat c_p shows a flat peak at $\simeq 120°$ C (Fig. 3b). The shaded area in the figure corresponds to a heat of transition of ~ 40 J (g atom)$^{-1}$.

No anomalies in thermal expansion were found in any of the experiments carried out between room temperature and 600° C using heating and cooling rates between 1 and 10 K min^{-1}. The coefficient of thermal expansion deduced from these experiments was $\alpha_{20-300°C} = (13.5 \pm 0.5) \times 10^{-6}$ K^{-1}.

Elasticity data were difficult to obtain due to the poor quality of the samples and the high internal friction. Room temperature values of Young's modulus varied between 0.9 and 1.1×10^{10} N m^{-2} for different specimens and according to the method of measurement. It is well known that Al–Ca alloys containing up to 30 vol% Al_4Ca exhibit a drastic decrease of modulus with increasing Ca content [2–5, 8]. Extrapolating these results to 100 vol% Al_4Ca, our values, as well as the value given earlier, [2], lie within the limits of accuracy of this procedure such that no decision can be made as to which value is correct.

The temperature dependence of Young's modulus, as obtained with the resonance method, is drawn in Fig. 3c. With increasing temperature, the modulus decreases between $\sim -180°$ C and $\sim 0°$ C, followed by a slight, but qualitatively reproducible peak.

Above 100° C, a pronounced increase is observed. On cooling, we were not able to obtain reproducible results below 300° C due to high internal friction.

Comparing the ρ-, c_P- and $E(T)$-curves of Fig. 3, the upper limit of the anomalies lies at $\simeq 130°$ C. A lower limit may be set at $\simeq -30°$ C from the first observable changes in slope of $\rho(T)$ and of $E(T)$. Unfortunately, we were not able to obtain quantitative results of c_P in this low temperature region. However, some DSC curves showed an anomaly at $\simeq -30°$ C, too. Therefore, a second phase transition may possibly occur below room temperature, but we did not investigate this temperature region further.

4. Structure

4.1. X-ray spectrum

Parts of the X-ray spectrum obtained at room temperature with the slowly cooled sample are given in Fig. 4. Most lines are split, indicating a lower than tetragonal symmetry. Indexing with a

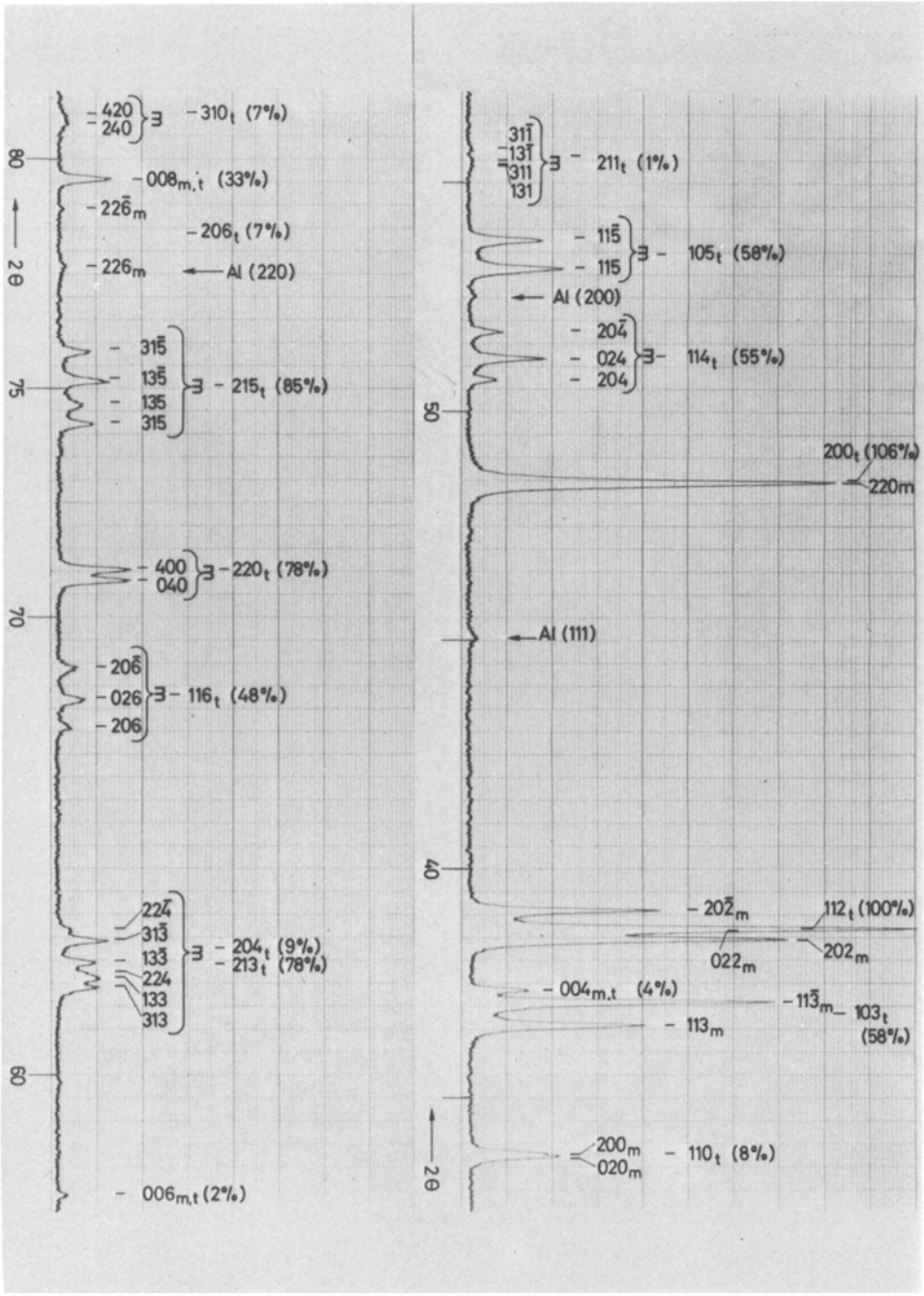

Figure 4 Room temperature X-ray spectra of Al_4Ca, obtained with Co$K\alpha_1$-radiation. Calculated 2θ values for the monoclinic unit cell are termed m, for a tetragonal symmetry termed t. nF^2 values given are calculated for tetragonal symmetry and scaled to 100% for the $(1\,1\,2)_t$-line.

tetragonal unit cell, as suggested by Nowotny *et al.* [1], is only possible if the additional splitting is neglected. This indexing is termed "t" (tetragonal) in Fig. 4; "best" agreement was obtained with lattice parameters $a_t = 0.4354$ nm, $c_t = 1.118$ nm, i.e. slightly different values than those given by Nowotny *et al.* No complete calculation of the intensities was performed: the values given in Fig. 4 are proportional to nF^2 (n = multiplicity factor, F = structure factor (rough estimate only)) and scaled to 100% for the $(1\,1\,2)_t$ line.

However, the split lines in Fig. 4 can be fully

accounted for by assuming a small distortion of the tetragonal cell to monoclinic symmetry with the following lattice parameters: $a = 0.6158$ nm, $b = 0.6175$ nm, $c = 1.118$ nm, $\beta = 88.9°$. The calculated 2θ values for this unit cell are marked "m" (monoclinic) in Fig. 4.

A spectrum recorded at 170° C did not show any monoclinic line splitting and could be indexed on the basis of the tetragonal unit cell. The lattice parameters deduced from this spectrum were consistent with the (tetragonal) values a_t, c_t given above obtained by using the thermal expansion coefficient deduced from dilatometry. This confirms that only a minor volume change or none at all is associated with the transformation, as suggested by the absence of a dilatometric anomaly.

The line intensities of the spectrum taken at 170° C were consistent with the Dl_3 structure, and as no drastic change was observed for the corresponding lines at room temperature (taking into account the change in multiplicity for monoclinic symmetry), we conclude that the atomic arrangement is not altered appreciably by the transformation. The monoclinic cell might be related to the tetragonal cell through $a_m \simeq \sqrt{2}a_t$ and $b_m \simeq \sqrt{2}a_t$ pointing in $(1\,1\,0)_t$ and $(1\,\bar{1}\,0)_t$ directions, respectively, and c_m tilted 1.1° from c_t in a $(1\,1\,0)_t$ plane.

The room temperature spectra of two samples annealed for 1 day at 160° C and 90° C, respectively, and quenched into ice-water, both showed the features of Fig. 4. No traces originating from untransformed material were observed in these spectra.

4.2. Electron microscopy

A great variety of fine structure is present within the lamellae of $\simeq 1\,\mu$m width visible in Figs. 1 and 2.

Slowly cooled samples gave stable EM images at room temperature. Using a heating holder, all of these lamellae disappeared on heating and reappeared gradually on cooling to room temperature, but mostly on a finer scale.

In quenched samples, the influence of the electron beam leads to the motion of boundaries as well as to a "burst-like" disappearance of very small ($\lesssim 0.1\,\mu$m) lamellae. These instabilities were confined to a narrow region near the edge of the foils. As an example, Figs. 5a and b show the same specimen area in an interval of few seconds; they reveal changes of an interface which was exposed to the electron beam for the first time. Under the heating influence of the beam, the zig-zag boundary configuration relaxes to a straight boundary approximately parallel to the foil-edge at a rate of $\simeq 0.1$ m sec^{-1}.

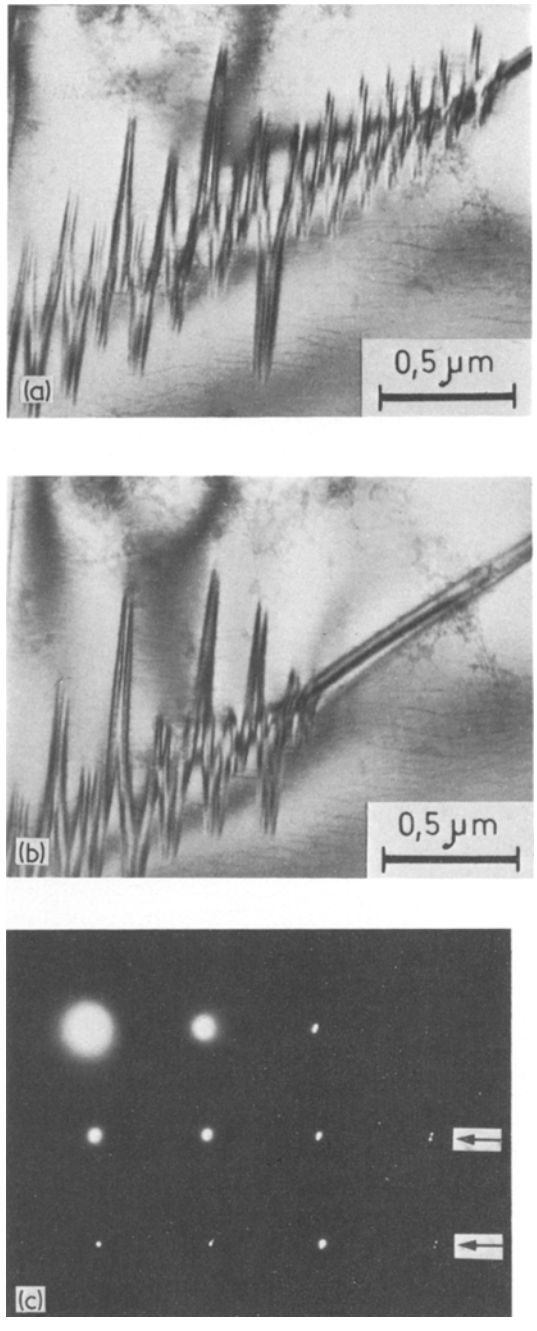

Figure 5 Quenched sample exposed for the first time to the electron beam. Relaxing zig-zag boundary, (b) is taken from the same area a few seconds later; (c) corresponding DP. [0 0 1] zone (with split spots marked by an arrow).

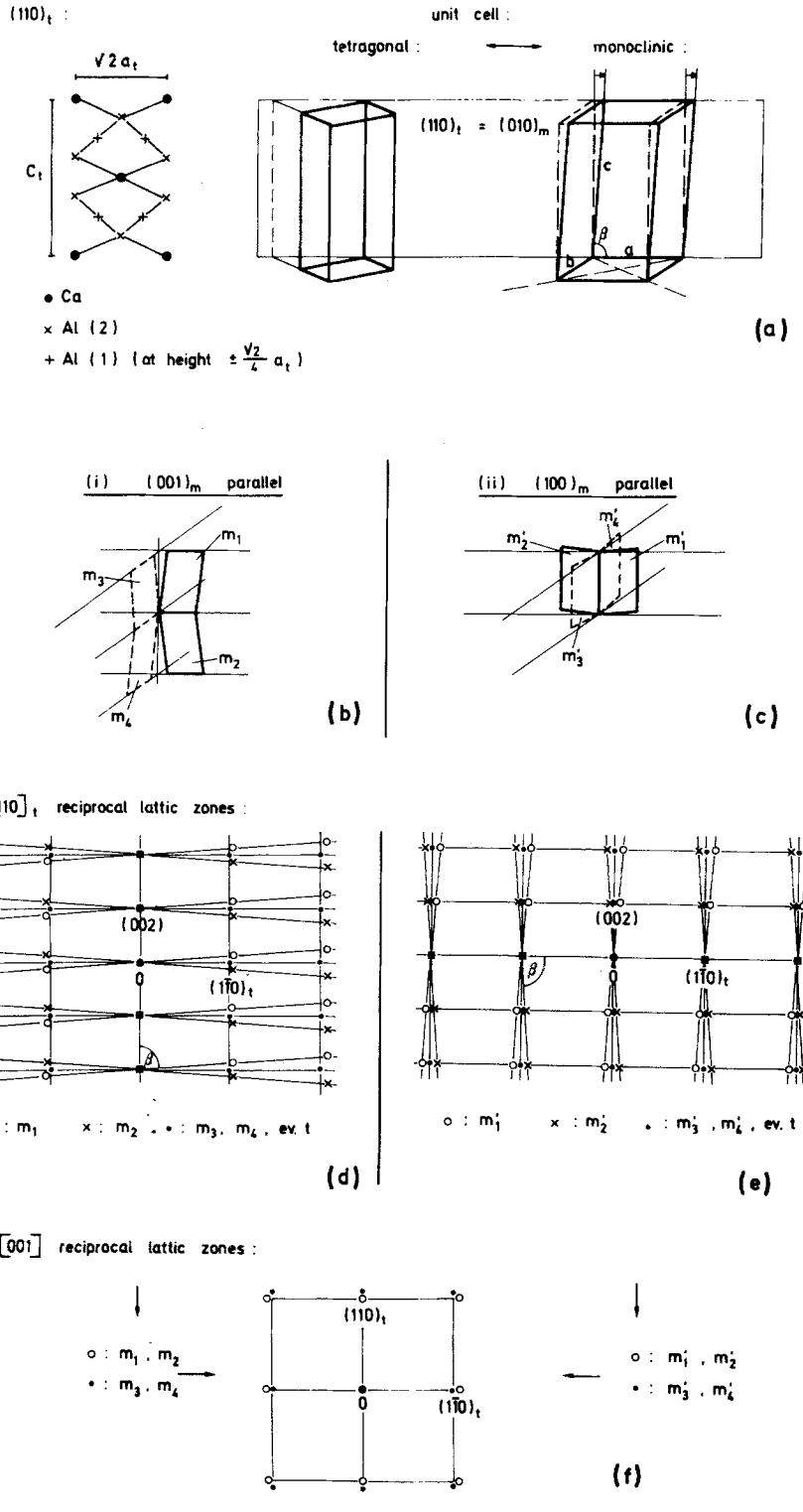

Figure 6 (a) Atomic positions of the $1\,1\,0_t$-plane, corresponding tetragonal unit cell and monoclinic cell. (b) Orientational variants $m_1 \ldots m_4$ if $(0\,0\,1)$-planes remain parallel during the transformation. (c) Orientational variants $m'_1 \ldots m'_4$ if $(1\,1\,0)_t \sim (1\,0\,0)_m$-planes remain parallel during the transformation. (d) $[1\,1\,0]_t$ reciprocal lattice zones for variant (i) resulting in split spots (see text), exaggerated. (e) As in (d) but for orientational variants (ii). (f) [0 0 1] reciprocal lattice zones, identical for case (i) and (ii), exaggerated.

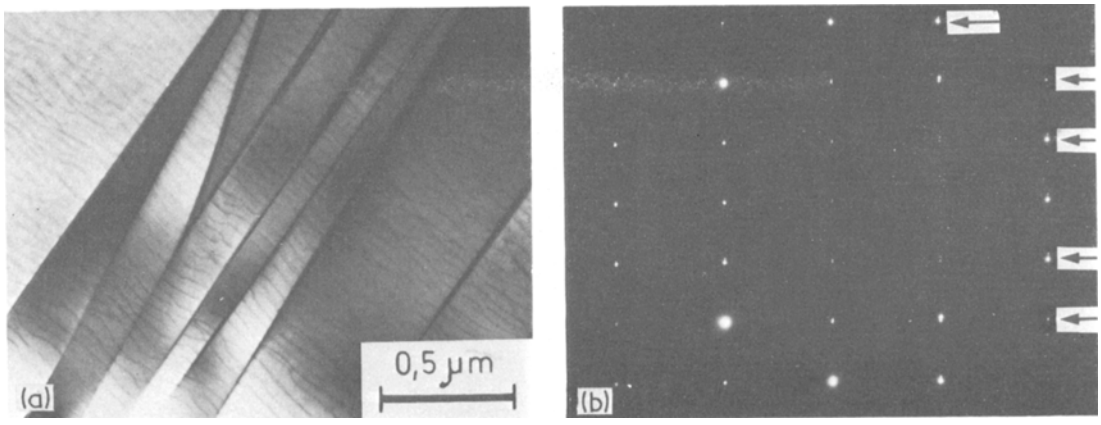

Figure 7 $[1\,\bar{1}\,0]_t$-pattern corresponding to orientational variant (i), spots split 3-fold are marked by an arrow. Slowly cooled sample (a) microstrucutre; (b) corresponding diffraction pattern.

5. Orientational relationships

In what follows we use the tetragonal indices of the Dl_3 structure to describe the "rough geometry" of the EM-images; the monoclinic symmetry is taken into account only where the fine features (split spots) of the diffraction patterns are to be analysed.

Assuming the transformational shear mechanism of $(1\,1\,0)_t$-planes to $(1\,0\,0)_m$-planes already mentioned, the most simple orientational relationships for a completely transformed material are drawn in Fig. 6. From the symmetry of the tretragonal cell, 4 monoclinic orientational variants are possible. In (i) (Fig. 6b), it is assumed that (0 0 1)-planes remain parallel. Then, the two variants marked m_1 and m_2 with shear direction parallel to the drawing plane of Fig. 6b are twin related with (0 0 1)-twinning plane, whereas the other two variants m_3 and m_4 with shear perpendicular to the drawing plane, form another equivalent twin pair. In (ii) (Fig. 6c), it is assumed that $(1\,1\,0)_t = (1\,0\,0)_m$-planes remain parallel, resulting in two other pairs (m_1', m_2') and (m_3', m_4') with $(1\,0\,0)_m$ twinning plane. Constructing the reciprocal lattice zones $(1\,\bar{1}\,0)_t$ for these two cases, the patterns of Figs. 6d and e are obtained. (Note that not all points lie exactly in these zones, e.g. in Fig. 6d, the zones corresponding to m_3 and m_4 points are tilted $+1.1^\circ$ along the (0 0 1)-row and fall approximately together with the corresponding tetragonal reciprocal lattice points in this projection.)

Both of these patterns were found experimentally, (i) in slowly cooled samples (Fig. 7) and

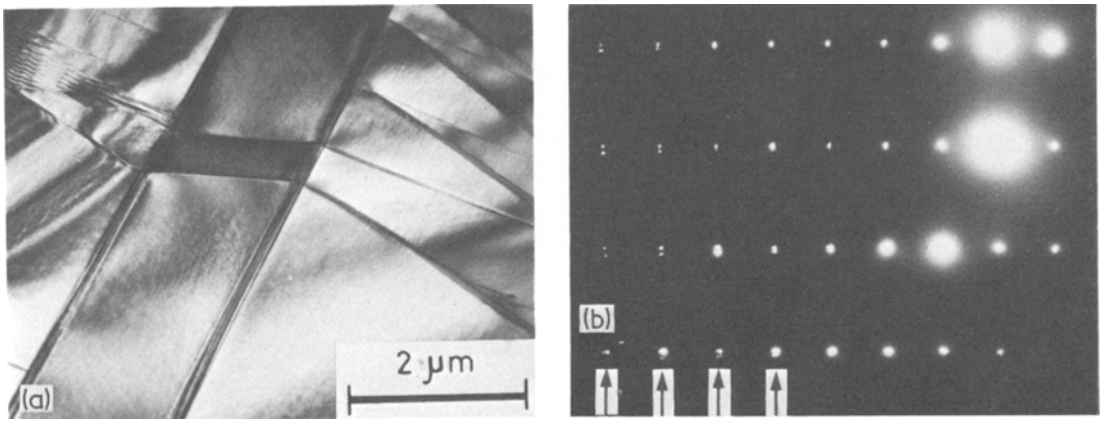

Figure 8 $[1\,\bar{1}\,0]_t$-pattern split spots of variant (ii). Showing two fold splitting m_1' and (m_3', m_4'), some spots are split up to 4-fold corresponding to both orientational variants (i) and (ii). (a) Microstructure; (b) corresponding diffraction pattern.

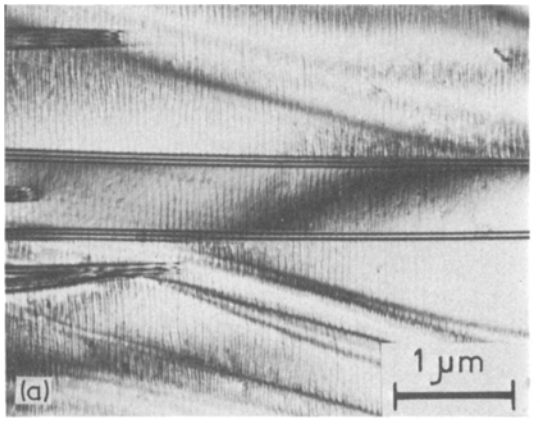

Figure 9 $[0\bar{2}1]_{\text{parent}}$ and $\simeq[023]_{\text{twin}}$ pattern corresponding to a possible twin system with $(0\bar{1}5)_t$-twinning plane. (a) Microstructure; (b) corresponding diffraction pattern.

(ii) in a quenched sample (Fig. 8). In some cases, both variants were present in the same image (Fig. 8). The magnitude of the splitting as determined from these photographs yielded $\beta = 88.9 \pm 0.15°$ and $(b-a)/a = 0.003 \pm 0.001$, in agreement with the lattice parameters derived from the X-ray spectra. Some, but not all, boundaries of the corresponding bright-field images of Figs. 7 and 8 are consistent with a composition plane equal to the twinning plane, i.e. $[100]_m \sim [110]_t$-direction (intersection of a (001)-twinning plane) in Fig. 7

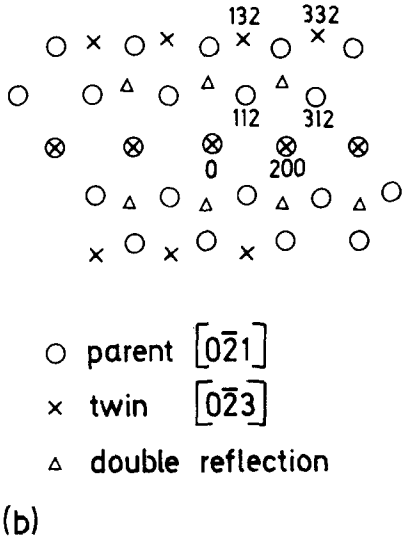

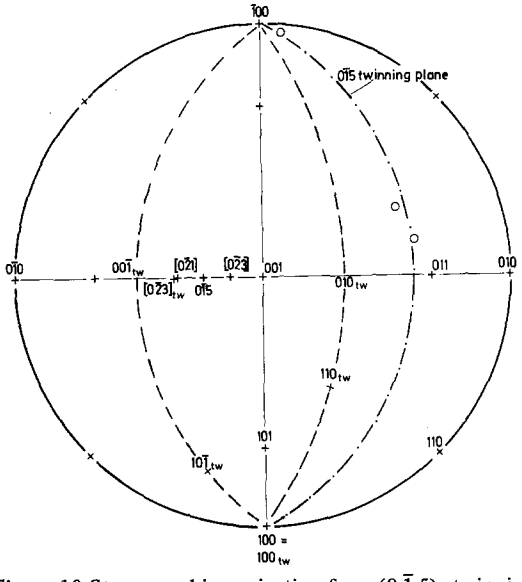

Figure 10 Stereographic projection for a $(0\bar{1}5)_t$-twinning place geometry. Indices corresponding to the twin are marked "tw". Trace analysis of the composition plane of the same area of Fig. 9, using different tilt angles, are given by open circles.

and [001]-direction (intersection of $(100)_m \sim (110)_t$-twinning plane) in Fig. 8.

The calculated [001]-reciprocal lattice zone is drawn in Fig. 6f and is identical for both cases (i) and (ii) (neglecting the small tilt of ± 1.1° for some orientational variants). The splitting obtained in this projection is too small to be observable in our EM-diffraction patterns. This behaviour was observed in some slowly cooled samples; however, some quenched samples showed a definite splitting in [001]-orientation (e.g. in Fig. 5c) which is in contradiction to Fig. 6f. This splitting indicates a rotation of at least 1° of $(100)_m$ or $(010)_m$ planes from orthogonal and can be explained only if other orientational variants than given in Fig. 6 are allowed. $[1\bar{1}0]$-patterns are not observably affected by such a small rotation As all other split diffraction patterns we obtained from numerous other zones,

other than [001], were explainable as being within experimental scatter with (i) or (ii), we did not attempt to establish other orientation relationships.

In some instances, a high angle orientation relationship was found, too. Fig. 9a shows the microstructure and Fig. 9b the corresponding diffraction pattern of an example. Neglecting the monoclinic distortion, this orientational relationship can be ascribed to another twin system. As indicated in the lower part of Fig. 9b, the orientations of the parent and twin are approximately $[0\bar{2}1]_t$ and $[0\bar{2}3]_t$, with a common (100) reciprocal lattice direction in this figure. The corresponding twinning plane is then approximately $K_1 \simeq (0\bar{1}5)_t$.

Fig. 10 shows the corresponding geometry in a stereographic projection. Trace analysis of the composition plane using different tilt angles is indicated in this figure, too, showing that the composition plane is approximately equal to the twinning plane. Assuming rational twinning elements, it follows from symmetry arguments [9] that the plane of shear is $(100)_t$ ($\eta_1 = [0\bar{5}1]_t$). η_2 is then tentatively determined as a low indexed direction parallel to the shear plane and forming an angle ψ near 90° with $\eta_1 : \eta_2 = [011]_t$ with $\psi = 84.5°$. However, if the monoclinic distortion is taken into account, it is not possible to decide from our data if this orientation relationship corresponds to an "exact" twin system or to a relationship with only "approximate" twin geometry.

Several other orientation relationships were found which were inconsistent with both the low angle twin variants (i) and (ii) and the high angle variant just described.

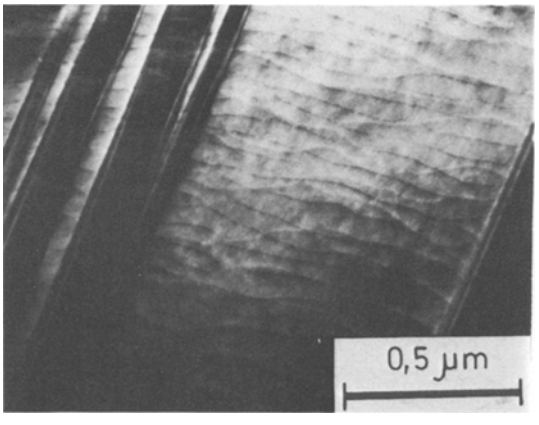

Figure 11 Growth faults in Al_4Ca. Dark-field image with operating reflection $(2\bar{2}0)_t$. (DF $(2\bar{2}0)_t$). Dark and bright contrast of faults.

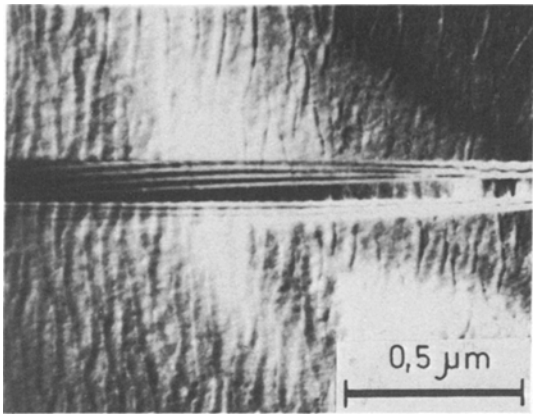

Figure 12 Growth faults in Al_4Ca (DF $(020)_t$). Dark and bright ribbons of combined faults.

These may be due to still further twin systems, mixtures of the twin systems described, or incidental composition planes of neighbouring crystallites.

6. Growth faults

The electron microscopic images show a contrast effect which continuously penetrates the lamellae described in the previous sections. Only the contrast effect itself is affected depending on the relevant lattice distortion. Therefore, the lattice defects causing this contrast must be present before the tetragonal–monoclinic transformation took place. In order to clarify the nature of these defects dark-field electron microscopy with different reflections operating was used. A contrast effect was observed in all dark-field images taken. However, the nature and the intensity of the contrast varied considerably. Going along the $[001]_t$ reciprocal lattice direction the contrast is very weak for the $(002)_t$, $(006)_t$ reflections and strong for the $(004)_t$, $(008)_t$ reflections. Because of the close packing of this reciprocal lattice direction interference effects cannot be excluded and it may be that the contrast of the $(002)_t$ and $(006)_t$ images is anomalous.

There are at least two different sets of faults. This is seen from Fig. 11 (dark-field DF $(2\bar{2}0)_t$) where one set shows dark the other one bright contrast. The contrast of the faults is not uniform. There are bright and dark spots on it. The faults interact. This is seen from Fig. 12 (DF $(020)_t$)

where single faults are almost invisible but combined faults form black and white ribbons.

Some features of the faults are common with antiphase boundaries, for example the extinction in some reflections operating. But the non-uniformity of the contrast cannot be interpreted assuming simple antiphase boundaries. It may be that agglomerates of impurities or composition fluctuations (i.e. layers of wrong lattice site occupation) are the cause of the non-uniformity. Therefore the exact nature of the faults remains open. We conclude that they are growth faults introduced by a transformation during the preparation of the alloys at substantially higher temperatures than the tetragonal–monoclinic transformation.

7. Conclusions

The experimental results indicate that a martensitic transformation occurs in Al_4Ca with $M_s \simeq 130°$ and M_f slightly above room temperature. The structural change associated with the transformation is from a tetragonal to a monoclinic structure. The orientation relationships of the twin lamellae observed in the martensitic product are easily explained with a transformational shear of 1.1° in $(1\,1\,0)_t$ planes. The transformation is associated with anomalies of the specific resistivity, the specific heat and the elastic modulus. In particular the decrease of Young's modulus with decreasing temperature above M_s is characteristic of several types of martensitic transformations. The high internal friction found is typical for premartensitic and martensitic phenomena [10, 11]. In the thermal expansion no anomalies were detected. Hysteresis effects are small ($< 5°$ C). There is no correlation between the "brittle-to-ductile" transition of Al_4Ca at $\simeq 300°$ C and the martensitic transformation.

A second transformation may occur at $\simeq -30°$ C which we did not investigate in detail.

Acknowledgements

We thank Professor H. Warlimont for initiating this work and Drs G. Hausch, J. C. Jaquet and E. Török for stimulating discussions. The technical help of Messrs M. Koutny and B. Scalco is also acknowledged.

References

1. H. NOWOTNY, E. WORMNES and A. MOHRNHEIM, *Z. Metallkde.* **32** (1940) 39.
2. W. KÖSTER and W. RAUSCHER, *ibid.* **39** (1948) 111.
3. R. MATERA, G. PIATTI and K. N. STREET, *Aluminium* **49** (1973) 335.
4. G. PIATTI, G. PELLEGRINI and R. TRIPPODO, *J. Mater. Sci.* **11** (1976) 186.
5. J. C. JAQUET, Ph. D. Thesis, Stuttgart (1978).
6. H. ZOGG, J. TIMM and H. WARLIMONT, *Aluminium* (to be published).
7. G. HAUSCH and E. TÖRÖK, *Phys. Stat. Sol. (a)* **40** (1977) 55.
8. N. DUDZINSKI, *J. Inst. Metals* **81** (1952–3) 49.
9. R. W. CAHN, *Acta Met.* **1** (1953) 49.
10. L. DELAEY, E. AERNOUT and J. ROOS, *Metall.* **31** (1978) 1325.
11. H. WARLIMONT, G. HAUSCH, A. PRASETYO and F. REYNAUD, Proceedings 1 JIM International Symposium on "New Aspects of Martensitic Transformation", Kobe, Japan, 1976.

Received 11 October and accepted 17 November 1978.